Supporting Information

From Recombination Dynamics to Device Performance: Quantifying the Efficiency of Exciton Dissociation, Charge Separation and Extraction in Bulk Heterojunction Solar Cells with Fluorine-Substituted Polymer Donors

Julien Gorenflot, Andreas Paulke, Fortunato Piersimoni, Jannic Wolf, Zhipeng Kan, Federico Cruciani, Abdulrahman El Labban, Dieter Neher, Pierre M. Beaujuge, Frédéric Laquai**

Contents

S1. Summary of the device performances, reproduced from Ref [S1] 2

S2. Detailed flowchart of the methodology for individual yields determination 3

S3. Transient absorption spectra of [2H]T based blends 4

S4. Reference spectra used for spectra deconvolution 5

S5. Generation kinetics in [2H]T-based blends 7

S6. Nonlinear TA response at high fluences 8

S7. Ellipsometry measurements 10

S8. Transfer matrix simulations 12

S9. Optimized layer thickness 13

S10. "Two–pool" model parametrization of the charge carrier population decay[S7] 14

S11. "Two-pool" model fits for blends processed without solvent additives 19

S12. Charge carrier extraction time 20

S13. EQE spectra of blends processed without solvent additives 22

S14. E_{CT}-determination fit parameters 23

References 24

S1. Summary of the device performances, reproduced from Ref [S1]

Table S1. Photovoltaic performance of the polymer blends with $PC_{71}BM$ [a)] reproduced from Wolf et al. 2015.[S1]

Polymer	Add.[b)]	J_{SC} [mA cm^{-2}]	V_{OC} [V]	FF [%]	Avg. PCE	Max. PCE
P3HT	N	10.0	0.60	64	3.8	4.0
[2H]T	N	4.3	0.79	66	2.1	2.2
[2H]T	5%	5.7	0.79	60	2.3	2.7
[2F]T	N	8.6	0.90	69	5.2	5.4
[2F]T	5%	10.7	0.90	72	6.8	7.0

[a)] Devices with optimized [2X]T:$PC_{71}BM$ ratio of 1:1.5 (wt/wt) solution-cast from chlorobenzene (CB), and P3HT:$PC_{71}BM$ ratio of 1:1 (wt/wt) cast from dichlorobenzene (DCB); average values across 10 devices (device area: 0.1 cm^2). [b)] Devices prepared from solutions containing 5% (v/v) of the processing additive 1-chloronaphthalene (CN).

S2. Detailed flowchart of the methodology for individual yields determination

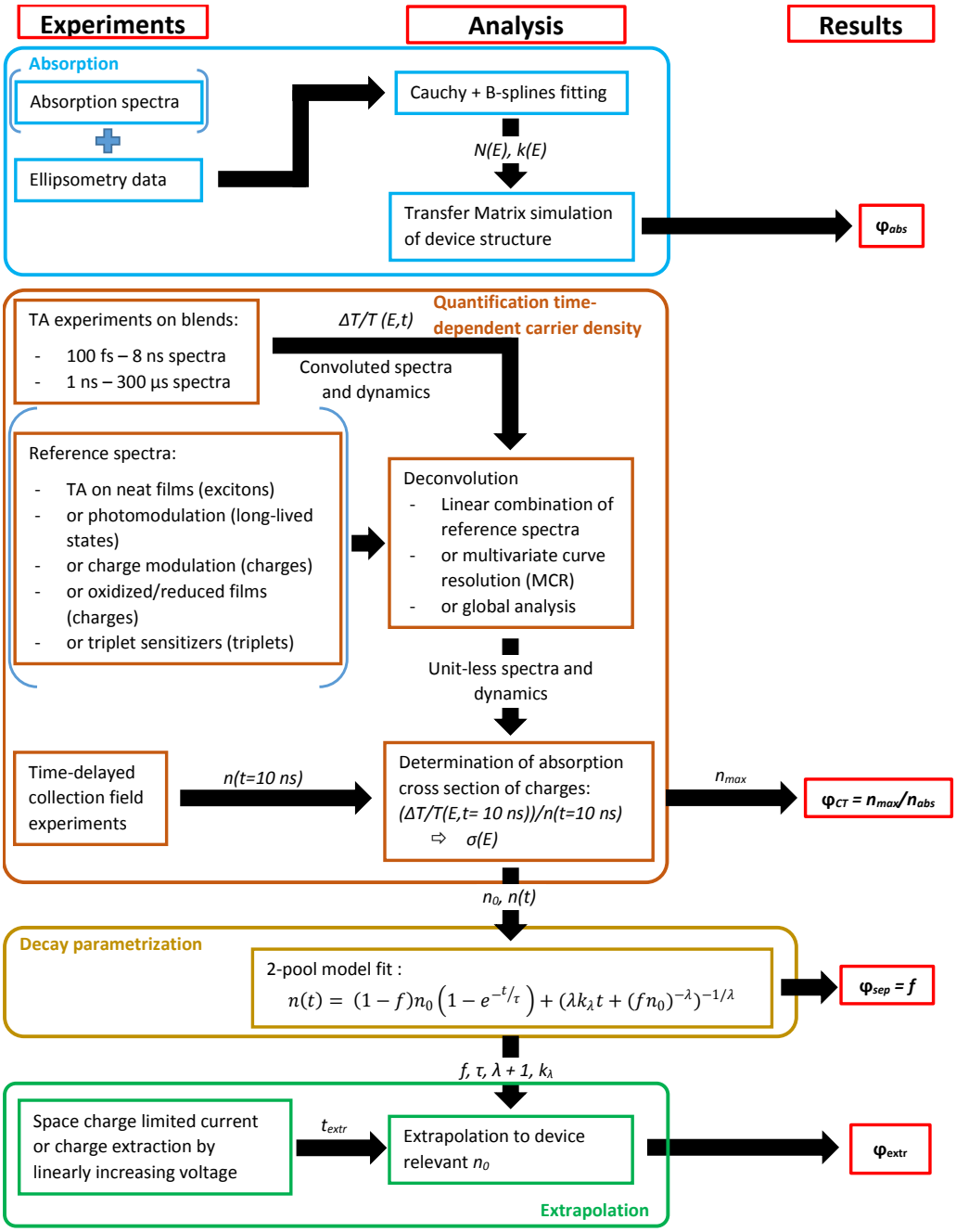

Figure S1. Detailed flowchart for the determination of the absorption, charge transfer, charge separation and charge extraction yields. *N* and *k* represent the real and imaginary parts or the refractive index, respectively. *E* is the probing energy (wavelengh), $\Delta T/T$ is the TA signal: the relative change in transmission upon pulsed photoexcitation, *n* is the charge density and n_0 its maximal/initial value, σ the absorption cross section. *f* is the fraction of separated charges, τ the lifetime of bound charge pairs, and k_λ the empirical coefficient for non geminate recombination of apparent order $\lambda+1$.

S3. Transient absorption spectra of [2H]T based blends

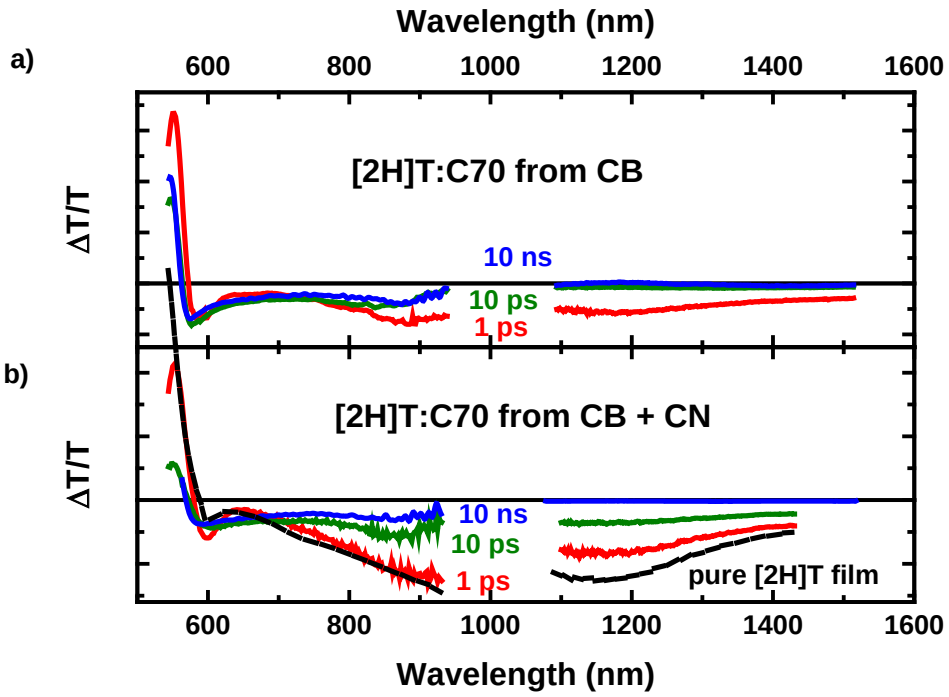

Figure S2. TA spectra of [2H]T:$PC_{71}BM$ (1:1.5) thin film blends prepared with and without CN as additive and excited at 532 nm with 10-11μJcm^{-2}pulse^{-1}. The dashed lines correspond to the early-time (0.5-0.6 ps) spectrum of a neat [2H]T polymer film for comparison.

S4. Reference spectra used for spectra deconvolution

The unit-less kinetics $A_{excitons}(t)$ of excitons and $A_{charges}(t)$ of charges were obtained by deconvoluting their contribution to the spectra at each time delay *t*:

$$\Delta T/T(t) = A_{excitons}(t) * S_{\text{exciton}} + A_{polarons}(t) * S_{polaron} \qquad \text{Equation S1}$$

The exciton reference spectra $S_{exciton}$ are equivalent to the normalized TA spectra of neat polymer films (processed from CB solution, 20 mg mL^{-1}) averaged between 10 and 100 ps for different fluences (from 1 to 13 µJ cm^{-2}). The charge-induced absorption spectra $S_{charges}$ were obtained from the normalized long delay TA spectra of the blends averaged between 10 and 500 ns for [2F]T-based blends and from 50 to 500 ns for [2H]T-based blends and for different fluences (from 1.5 to 64 µJ cm^{-2}). The spectra are shown in **Figure S3**. Note that the photobleach regions were excluded from the fits as those regions are affected by spectral relaxation[S2] and thus do not fulfil the required condition to remain constant over time. **Equation S1** is thus applied to a wavelength range from 575 to 1510 and 590 to 1510 nm for [2F]T-based and [2H]T-based blends, respectively.

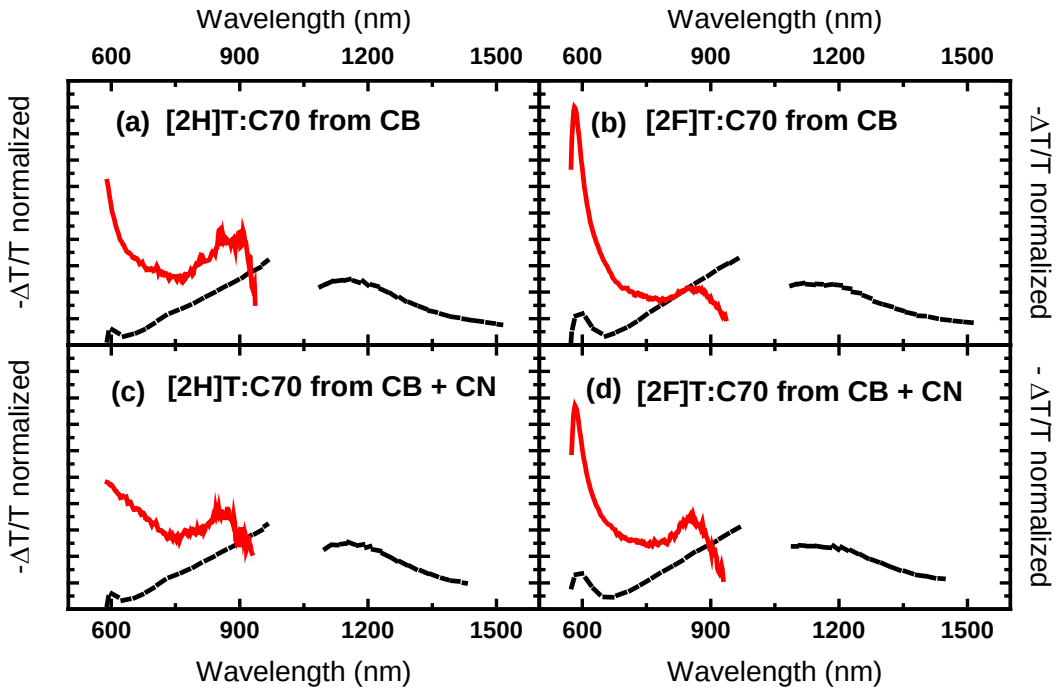

Figure S3. Reference spectra $S_{exciton}$ (back dashed line) and $S_{charges}$ (red continuous line) used for deconvoluting exciton and charge carrier contributions in blend TA spectra. No charge-induced absorption was observed at higher wavelengths. The spectra are normalized in surface area. The 570 – 940 nm and 1060 – 1510 nm regions of the spectra were obtained from separate measurements, thus their amplitude has been corrected for the fluence mismatch.

S5. Generation kinetics in [2H]T-based blends

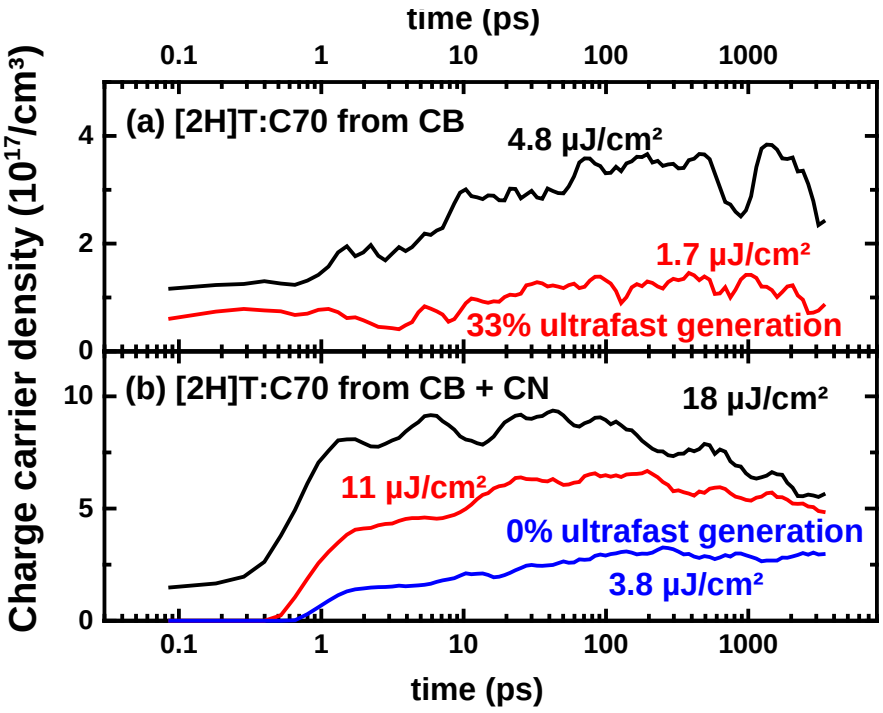

Figure S4. Charge carrier dynamics in [2H]T:$PC_{71}BM$ blends extracted by deconvolution of the TA spectra of films prepared without solvent additives (a) and with 5% (w/w) chloronaphtalene (b).

S6. Nonlinear TA response at high fluences

In neat polymer films we expect that each absorbed photon creates an exciton (in contrast to the bulk heterojunction which exhibits ultrafast charge generation at the D/A interface). This allows estimation of the exciton cross section by division of the exciton signal amplitude by the density of absorbed photons. However, during the excitation pulse duration, higher order, that is, non-linear processes such as exciton-exciton annihilation or exciton-charge annihilation can occur resulting in a sublinear increase of the density of excitons with fluence. As can be seen in **Figure S5**, no such sublinear fluence dependence was observed within the rise time of $\Delta T/T$ (typically 500 fs, which roughly corresponds to the pulse width, assuming a full width at half maximum of 120 fs). Note: exciton recombination to the ground state can be neglected on this timescale, as it is much slower (see Table 1).

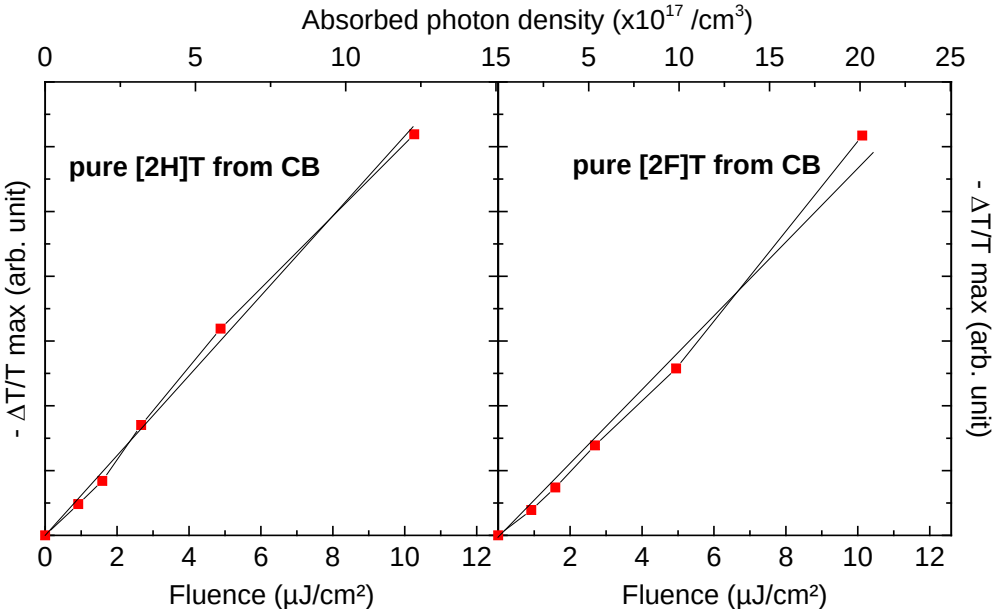

Figure S5. Amplitude of the exciton-induced absorption signal integrated over the whole 1060 – 1510 nm spectral range.

S7. Ellipsometry measurements

The active layer's optical constants *n* and *k* were determined by variable angle spectroscopic ellipsometry (VASE) using an M-2000 ellipsometer (J.A. Woolam Co., Inc). The active layers were cast on cleaned silicon substrates covered with different thicknesses of SiO_2 (51 nm and 70 nm). The VASE measurements were performed with incident angles varied between 45 and 75° relative to the samples. The data analysis software Complete Ease (J.A. Woolam Co., Inc) was used to process all collected data. The sample thickness *d* was first inferred by fitting a Cauchy dispersion relationship, $n(\lambda) = A + B/\lambda^2 + C/\lambda^4$ to the wavelength dependence of the reflectance ratio over the spectral range in which the material is optically transparent (900 – 1700 nm). The first coefficient *A* of the Cauchy equation was used as an estimate of the low frequency refractive index to determine the static relative dielectric constant ε_r of the material $\varepsilon_r = n^2$. This is essentially equivalent to neglecting any vibrational (ionic) contribution to the static dielectric function related to the material's absorption in the infrared. For comparison and reference: in a spin-coated film of a poly-arylene ether, Postava et al. have determined that the vibronic contribution accounts for only 0.08 of the static dielectric constant of 2.78. [S4]

Table S2. Static refraction indexes and corresponding relative dielectric constants estimated from the fit of a Cauchy dispersion relation to the wavelength dependence of the reflectance ratio over the spectral range in which the active layer is transparent (here: 900 – 1700 nm).

Material system	[2H]T:$PC_{71}BM$ from CB	[2H]T:$PC_{71}BM$ from CB + CN	[2F]T:$PC_{71}BM$ from CB	[2F]T:$PC_{71}BM$ from CB + CN
n_{static} [a)]	1.98	1.77	1.99	1.83
ε_r	3.92	3.13	3.96	3.35

A *B-splines* model was then applied across the full spectral range to extract the optical constants *n* and *k* represented in **Figure S6**. [S5]

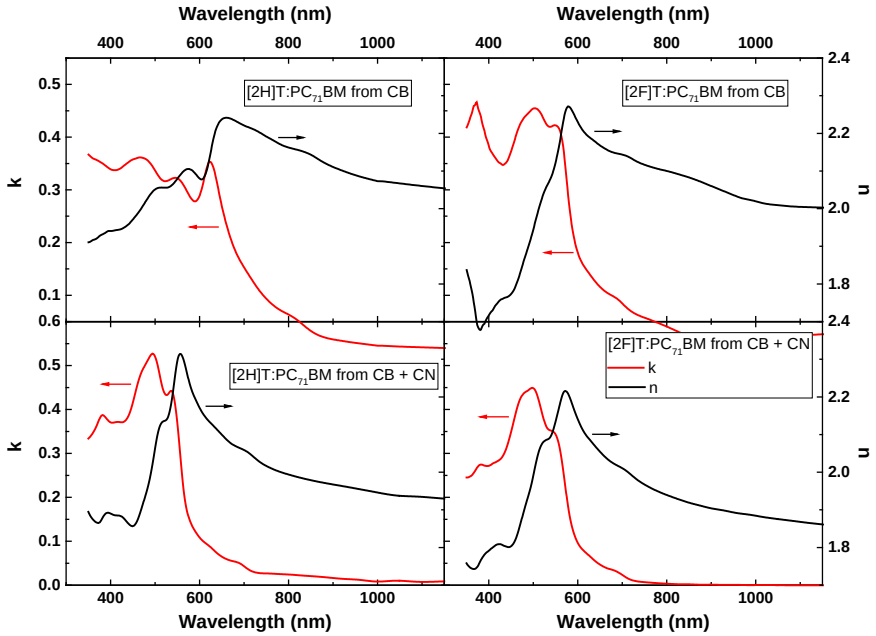

Figure S6. Optical indexes as extracted from fitting the wavelength dependence of the reflectance ratio to a *B-spline* model.

S8. Transfer matrix simulations

The optical indexes determined by ellipsometry were used as input to a transfer matrix model [S3] to calculate the fraction of the excitation light absorbed in the device structure used for the TDCF experiments as well as the optimal film thicknesses. The transfer matrix code used for these simulations was developed by George F. Burkhard and Eric T. Hoke. The code is freely available from: http://web.stanford.edu/group/mcgehee/transfermatrix/index.html and was adapted from the procedures originally described in Ref. [S3] and [S6].

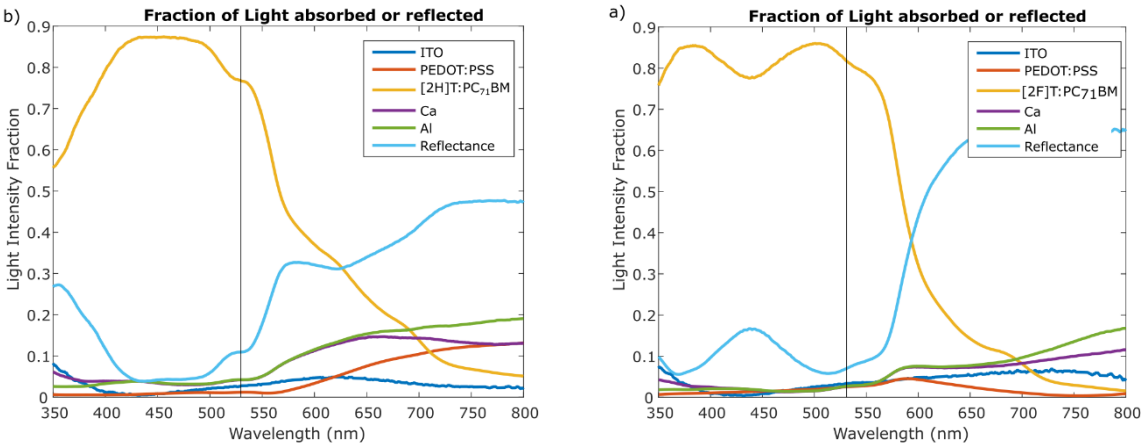

Figure S7. Fraction of incident light absorbed in the devices used for the TDCF experiment (a) SiO_2/ITO/PEDOT:PSS/PBDT[2H]T:PC_{71}BM/Ca/Al with layer thicknesses in nm: (0)/150/35/72/7/100. (b) SiO_2/ITO/PEDOT:PSS/[2F]T:PC_{71}BM/Ca/Al with layer thicknesses in nm: (0)/150/35/157/7/100. Note that the glass layer thickness being on a totally different range does not play any role in the transfer matrix simulation, and the reflection on its surface is neglected. The vertical line represents the excitation wavelength used in TDCF.

S9. Optimized layer thickness

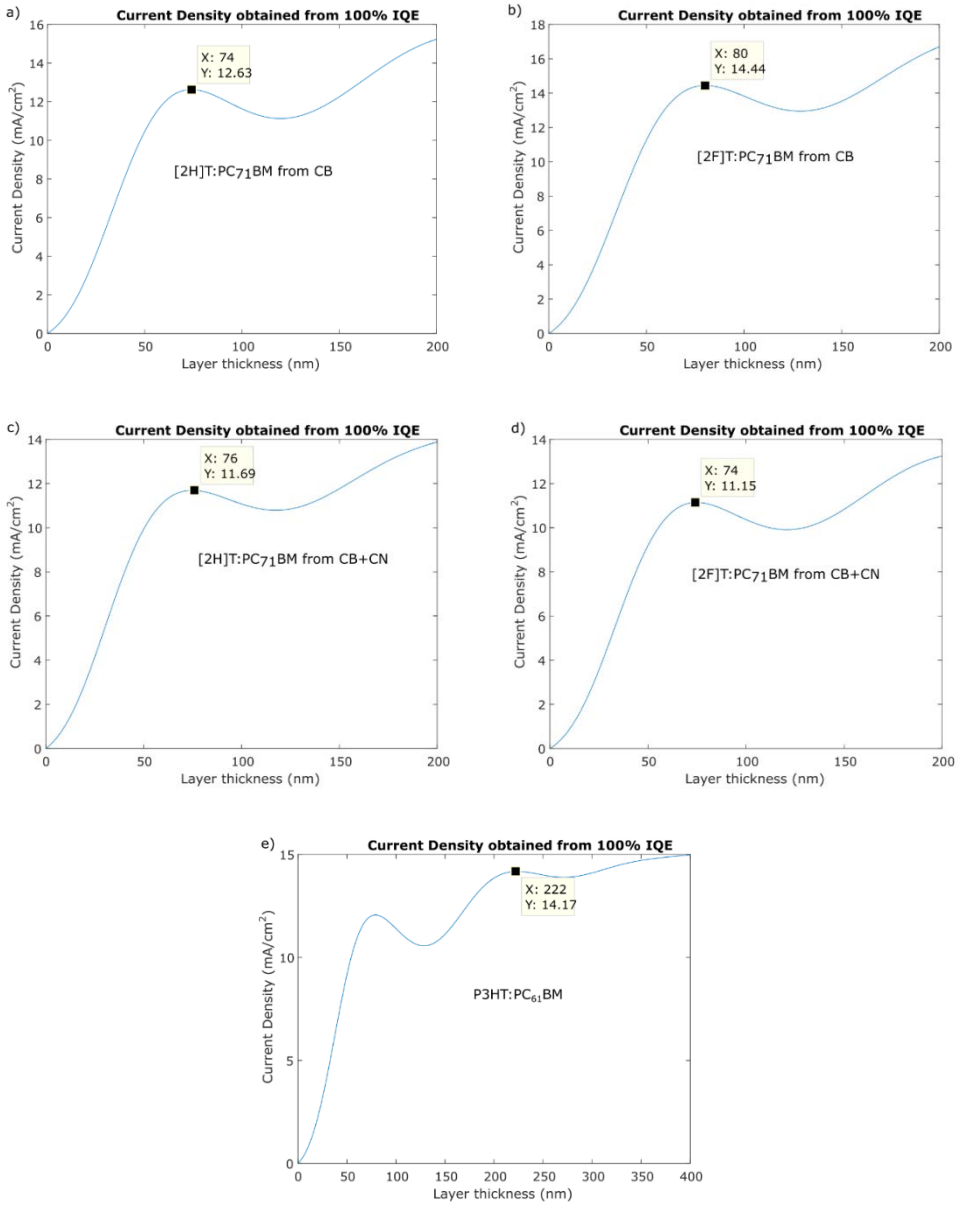

Figure S8. Thickness dependence of the short circuit currents calculated by transfer matrix simulations for devices of structures: SiO_2/ITO/PEDOT:PSS/active layer/Ca/Al with thicknesses in nanometers: (0)/110/35/x/7/100 assuming an internal quantum efficiency of

1. Except for P3HT:$PC_{61}BM$ the square represents the coordinates of the lowest thickness local optimum. Due to the limited hole mobilities in PBDT[2X]T, the local maxima corresponding to larger thicknesses are irrelevant. For P3HT:$PC_{61}BM$ the second lowest thickness maxima is considered, as for this blend the higher charge carrier mobility allows to use larger film thicknesses without losing charges by non-geminate recombination.

S10. "Two–pool" model parametrization of the charge carrier population decay[S7]

For each fluence *i* we determined an initial density $n_{0,i}$ of charges from the TA signal amplitude divided by the charge absorption cross section σ_{charge} as determined by comparison with TDCF data. We assume the charges are divided into two pools, namely a density $f \times n_{0,i}$ of spatially-separated (free) charges and a density $(1\text{-}f) \times n_{0,i}$ of coulombically-bound charges, that is, geminate pairs. For the recombination of these two carrier populations the following rate equations apply:

Coulombically-bound charges recombine geminately with an intrinsic lifetime τ:

$$\frac{d(1-f)n_i}{dt} = -\frac{(1-f)n_i}{\tau} \qquad \text{Equation S2}$$

while separated charges recombine non-geminately with an apparent recombination order $\lambda+1$ and a recombination prefactor k_λ:

$$\frac{dfn_i}{dt} = -k_\lambda (fn_i)^{\lambda+1} \qquad \text{Equation S3}$$

Above equations yield the following analytic solution:

$$n_i(t) = (1-f)n_{0i}\, e^{-t/\tau} + (\lambda k_\lambda t + (fn_{0i})^{-\lambda})^{-1/\lambda} \qquad \text{Equation S4}$$

Equation S4 was used to globally fit the charge-induced absorption decay across all fluences *i*, while the parameters *f*, τ, λ and k_λ were shared across all fluences. Note that at low fluence non-geminate recombination occurs at a later stage so that geminate and non-geminate recombination become sequential processes instead of parallel. This is reflected by a plateau in the dynamics of the charge carrier density between the time when most geminate charges have recombined and the time when the non-geminate recombination sets in. In this case, each of the parameters can be ascribed to a specific feature of the decay:

- n_0 is naturally the initial signal amplitude;
- τ governs the timescale of the first part of the decay (geminate recombination of bound charges);
- *f* is the value of the *y-axis* at which the plateau is observed in a normalized graph (i.e. it is equivalent to the fraction of charges left after geminate recombination has diminished the total carrier population);

- k_λ governs the onset of non-geminate recombination according to $t = (f n_{0i})^{-\lambda} / \lambda k_\lambda$, while the values of f, λ and n_o are determined by other features);
- λ is the asymptotic slope of the decay at long times on a log-log representation.

As a result, there is little room for parameters to vary, while still describing the experimental data. However, low fluences suffer from a poor signal-to-noise ratio, whereas at high fluences, geminate and non-geminate recombination become parallel processes.[S7] Employing a global fit across a range of fluences overcomes this problem.

Note that the non-geminate recombination prefactor k_λ extracted for two materials cannot be directly compared it is a function of λ (compare equation S3). In order to be able to compare the values, we reduced them to the equivalent bimolecular recombination prefactor k_2 according to:

$$k_2 n^2 = k_\lambda n^{\lambda+1} \qquad \text{Equation S5}$$

Using this approach, the value of k_2 becomes a function of the density of charges. In order to obtain a value with relevance for solar cells operating under one sun conditions, we use the density of charges $n = n_{1sun} = 5 \times 10^{15}$ cm^{-3} corresponding to the density of photons under a 1 sun illumination.

Thus:

$$k_2 = k_\lambda n_{1sun}^{\lambda-1}$$ Equation S6

For comparison the Langevin prefactor $k_{Langevin}$ can be calculated by:

$$k_{Langevin} = \frac{q}{\varepsilon}(\mu_e + \mu_h)$$ Equation S7

Here, the mobilities previously reported in Ref. [S8] and the relative permittivity as calculated from ellipsometry (see Ellipsometry section) were used to determine the Langevin prefactor.

Table S3. Dielectric constants, charge carrier mobilities, Langevin bimolecular recombination coefficients, experimentally observed high order recombination coefficient k_λ, bimolecular recombination coefficient computed from k_λ for n = 5×10^{-15} cm^{-3}, and calculated reduction coefficients.

Material system	ε_r	$\mu_e + \mu_h$ [$cm^2V^{-1}s^{-1}$]	$k_{Langevin}$ [$cm^{-3}s^{-1}$]	k_λ	k_2 [$cm^{-3}s^{-1}$]	$k_2 / k_{Langevin}$
[2H]T:PC71BM from CB	3.92	-	-	6.1×10^{-29}	3.1×10^{-13}	-
[2H]T:PC71BM from CB + CN	3.13	6.24×10^{-4}	3.6×10^{-10}	5×10^{-21}	6.4×10^{-12}	0.018
[2F]T:PC71BM from CB	3.96	-	-	4.8×10^{-25}	5.9×10^{-13}	-
[2F]T:PC71BM from CB + CN	3.34	7.35×10^{-4}	4×10^{-10}	9.2×10^{-23}	4.9×10^{-13}	0.0012
P3HT:PCBM	3.5	1×10^{-3}	5.1×10^{-10}	1.9×10^{-20}	1.2×10^{-13}	0.0002

S11. "Two-pool" model fits for blends processed without solvent additives

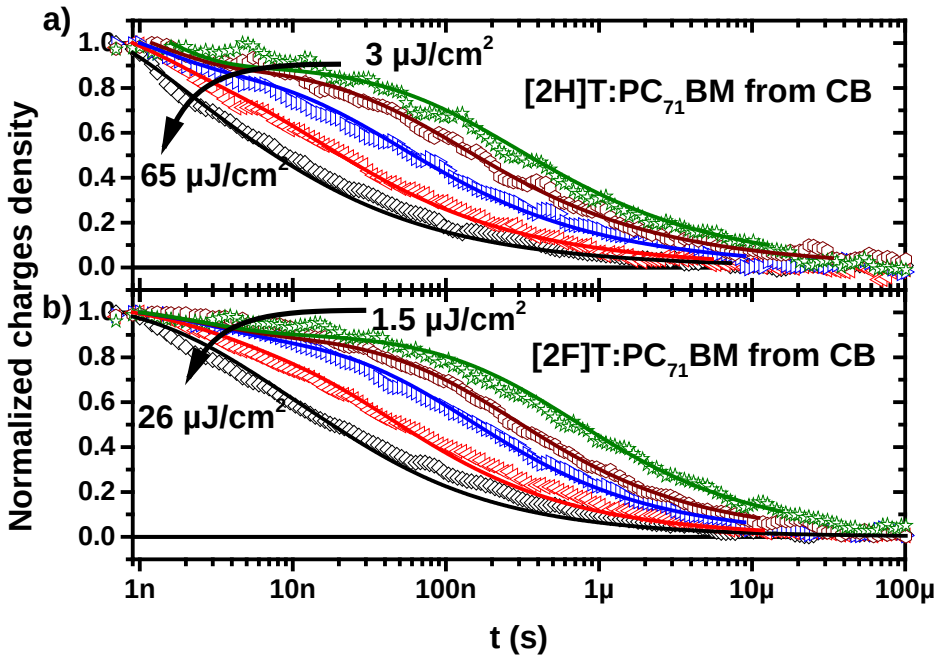

Figure S9. Charge-induced absorption decay dynamics in non-optimized (a) [2H]T:$PC_{71}BM$ and (b) [2F]T:$PC_{71}BM$ blends (open symbols) and fluence-dependent charge carrier recombination dynamics fitted by a two-pool model (solid lines). The dynamics were obtained from ns-μs transient absorption spectroscopy by averaging the optical response over the entire photoinduced absorption spectral range.

S12. Charge carrier extraction time

The extraction yield was approximated by $\varphi_{extr} = 1 - \varphi_{ng}$, where φ_{ng} is the fraction of separated charges recombining before charge extraction. The extraction time was estimated separately for electrons and holes as the dwell time required to drift-diffuse through the photoactive layer driven by an internal field corresponding to short circuit conditions in a device (considering a uniform field across the device photoactive layer and neglecting the voltage losses at the electrodes and in the PEDOT:PSS layer) using the mobilities measured in blends by space charge-limited current measurements (as published in Ref. [S8]). The results are summarized in table S4.

$$t_{\text{extraction}} = \frac{d}{\mu \times F} = \frac{d^2}{\mu \times V_{OC}} \qquad \text{Equation S7}$$

Table S4. Parameters used to calculate the extraction times.

Material system	d [a)] [nm]	Voc [V]	μ_e [b)] [$cm^2V^{-1}s^{-1}$]	μ_h [b)] [$cm^2V^{-1}s^{-1}$]	t_e	t_h
[2H]T:$PC_{71}BM$ from CB	74	0.79	-	-	-	-
[2H]T:$PC_{71}BM$ from CB + CN	74	0.79	6.2×10^{-4}	4.4×10^{-6}	112 ns	16 µs
[2F]T:$PC_{71}BM$ from CB	81	0.9	-	-	-	-
[2F]T:$PC_{71}BM$ from CB + CN	75	0.9	6.8×10^{-4}	3.5×10^{-5}	92 ns	1.8 µs
P3HT:PCBM	222	0.6	1×10^{-4} – 1×10^{-3}	1×10^{-4})	0.82 – 8.2 µs	8.2 µs

[a] See figure S8. [b] Space Charge Limited Current mobilities from Kan et al.[S8]. Time of Flight mobilities for a 1:1 wt. ratio P3HT:$PC_{61}BM$ from Baumann et al. and Mauer et al.[S9].

S13. EQE spectra of blends processed without solvent additives

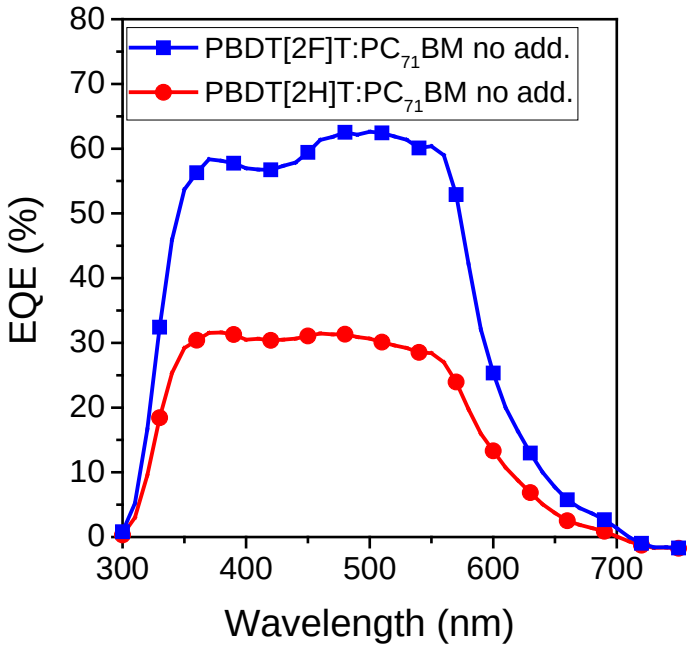

Figure S10. EQE spectra of blends processed without solvent additives.

S14. E_{CT}-determination fit parameters

The charge transfer state energy was determined from the CT-state absorption in the EQE spectra and the CT-state emission obtained by electroluminescence spectroscopy. More precisely, as previously shown by Vandewal et al.,[S10] the CT-state contributions to the device electroluminescence (*EL*) spectrum and photon-to-electron external quantum efficiency (*EQE*) can be expressed as follows:

$$EQE_{\mathrm{CT}} \times \mathrm{E} = \frac{f}{\sqrt{4\pi\lambda kT}} e^{\frac{-(E_{CT}-\lambda-E)^2}{4\lambda kT}} \qquad \text{Equation S8}$$

$$\frac{EL_{CT}}{E} = \frac{A}{\sqrt{4\pi\lambda kT}} e^{\frac{-(E_{CT}+\lambda-E)^2}{4\lambda kT}} \qquad \text{Equation S9}$$

Here *E* denotes the photon energy, *f* and *A* are factors proportional to the coupling between the two electronic states involved in the transition, λ is the reorganization energy associated with the transition, *kT* is the thermal energy and E_{CT} is the free-energy difference between the charge-transfer complex ground state and the CT excited state, the so-called *CT-state energy*. Both, emission and absorption spectra were measured on the same devices and the fits were performed globally for emission and absorption with the system-dependent parameters E_{CT} and λ being shared between both spectra. The fits are shown in Figure 11 and the extracted parameters in **table S5**. The parameter A is not calculated as the absolute quantum efficiency of the electroluminescence was not measured.

Table S5. CT-state energy: fit parameters.

Material system	f [eV^2]	E_{CT} [eV]	λ [eV]
[2H]T:PC71BM from CB + CN	4×10^{-4}	1.31	0.3
[2F]T:PC71BM from CB + CN	8.9×10^{-4}	1.36	0.35
P3HT:PCBM [a)]	8.8×10^{-5}	1.14	0.27

a) From ref. [S10]

References

[S1] J. Wolf, F. Cruciani, A. El Labban, P. M. Beaujuge, Chem. Mater. **2015**, *27* (12), 4184.

[S2] A. Melianas, F. Etzold, T. J. Savenije, F. Laquai, O Inganäs, M. Kemerink, *Nat. Commun.* **2015**, *6*, 8778.

[S3] L. Pettersson, L. Roman, O. Inganäs, *J. Appl. Phys.* **1999**, *86*, 487.

[S4] K. Postava, T. Yamaguchi, M. Horie, *Appl. Phys. Lett,* **2001,** *79* (14), 2231.

[S5] B. Johs, J. Hale, *Phys. Stat. Sol.* **2008**, *205*, 715.

[S6] P. Peumans, A. Yakimov, S. R. Forrest., *J. Appl. Phys.*, **2003**, *93* (7), 3693

[S7] I. A. Howard, R. Mauer, M. Meister, F. Laquai, *J. Am. Chem. Soc.* **2010**, *132*, 14866.

[S8] Z. Kan, A. Clulow, M. Babics, A. El Labban, D. Zhang, N. Wei, A. Nelson, F. Cruciani, S. Liu, P. Bern, I. R. Gentle, P. Beaujuge, The impact of fluorine substituent on the charge

generation, recombination and vertical phase segregation in bulk heterojunction in organic solar cells, *in preparation*.

[S9] (a) A. Baumann, J. Lorrmann, C. Deibel, V. Dyakonov, *Appl. Phys. Lett.* **2008**, *193*, 252104; (b) R. Mauer, M. Kastler, F. Laquai, *Adv. Funct. Mater.* **2010**, *20*, 2085-2092.

[S10] K. Vandewal, K. Tvingstedt, A. Gadisa, O. Inganäs, J. V. Manca, *Phys. Rev. B* **2010**, *81*, 125204.